Chain Length Effects on the Thermodynamic Properties of *n*-Alkane Crystals

Mark R. McGann and Daniel J. Lacks*

Department of Chemical Engineering, Tulane University, New Orleans, Louisiana 70118

Received: October 1, 1998

Molecular simulations are used to elucidate the effects of chain length on the unit cell dimensions, thermal expansion coefficients, heat capacities, and melting temperatures of *n*-alkane crystals. As the chain length increases, chain ends become less significant because they represent a smaller fraction of the chain, and the properties of the *n*-alkane crystals approach the properties of perfect polyethylene crystals. Energetic effects, associated with poorer packing at the chain ends, lead to a decrease in the density of shorter chain crystals. These energetic effects are compounded by entropic effects, associated with increased vibrational motion at chain ends, which lead to increased thermal expansion of shorter chain crystals. The heat capacity at constant volume is found to increase (on a per carbon basis) as chain length decreases, because shorter chains have more interchain modes in comparison to longer chains. Shorter chain crystals are also found to undergo instabilities related to melting at lower temperatures. The results presented here are expected to be qualitatively similar to the effects of lamellar thickness in semicrystalline polymers.

Introduction

The properties of semicrystalline polymer materials vary significantly with the processing conditions of the material. The dominant cause of these variations is the changing proportions of the crystalline and amorphous components. Processing conditions also influence the size of the crystallites, which affects material properties. The present paper addresses the crystallite size effects on material properties.

The crystalline regions of flexible polymer molecules are lamellar structures, with polymer chains oriented along the short dimension of the lamellae. The lamellar thickness, which is strongly dependent on processing conditions, influences the unit cell dimensions of polymer crystallites[1,2] and is estimated to have a significant impact on the heat capacity.[3] Also, the melting temperatures of semicrystalline polymers are not well defined and melting occurs over a range of several degrees;[4] the width and position of this temperature range are dependent on processing conditions, and this effect has been interpreted in terms of variations in crystallite size.[5]

The direct measurement of the dependence of these properties on lamellar thickness is difficult due to the amorphous regions present to some extent in all experimental samples.[6] Many studies have therefore focused on crystals of finite *n*-alkane molecules.[3,7,8] These crystals serve as models for crystalline polyethylene with lamellar thicknesses equal to the chain length and have the advantage of well-defined structures which allow for direct comparisons between different sets of experimental results and between experimental and simulation results.

The present investigation uses molecular simulations to elucidate the effects of lamellar thickness on the properties of polymer crystallites. Simulations of ideal polyethylene crystals are used to determine properties in the limit of large lamellar thickness, and crystals of small *n*-alkane molecules are used to determine properties in the limit of small lamellar thickness. The chain length dependence of the unit cell dimensions, thermal expansion coefficients, heat capacities, and melting temperatures of these materials are determined and interpreted in terms of the molecular-level interactions and dynamics.

Computational Method

Molecular simulations are carried out on *n*-alkane and polyethylene crystals as a function of temperature. The simulations are run for perfect infinite crystals in which all component atoms are explicitly modeled. The equilibrium lattice parameters at a given temperature are obtained as those that minimize the Helmholtz free energy, which is evaluated as the sum of the potential energy and the vibrational free energy obtained with a lattice dynamics method.

The potential energy is determined with the force field of Palmo et al.[9] This force field is designed to give accurate vibrational frequencies and is derived from a combination of theory and experiment. The nonbonded Coulombic and dispersion energies in the crystals are summed completely with Ewald methods.[10] Analytical first and second derivatives of the potential energy are calculated for use in geometry optimizations and normal-mode frequency calculations.

The vibrational free energy is determined in the quasi-harmonic approximation. This approximation is based on a Taylor expansion of the potential energy about the minimum, truncated after the quadratic term.[11] The dynamics of the crystal are reduced to that of uncoupled harmonic oscillators by a normal mode transformation (the normal-mode frequencies are obtained from the eigenvalues of the second derivative matrix). The quantum mechanical vibrational free energy (A_{vib}) for a set of M uncoupled harmonic oscillators with frequencies ω_i is known from statistical mechanics,

$$A_{\mathrm{vib}} = \sum_{i=1}^{M}\left[\frac{1}{2}\hbar\omega_i + kT\ln\left(1 - e^{\frac{-\hbar\omega_i}{kT}}\right)\right] \qquad (1)$$

Fourier space methods are used to determine the vibrational frequencies for modes occurring over more than one unit cell;[11] in this way, the effects of long wavelength vibrations are incorporated in the simulations. The total free energy is obtained by integration over the Fourier space wave vectors in the Brillouin zone; the integration is carried out using Gauss−Legendre quadrature with a 2 × 2 × 4 mesh (however, a 7 ×

10.1021/jp983932m CCC: $18.00
Published on Web 03/18/1999

7×7 Brillouin zone mesh is used to determine the stability of the final structures).

The heat capacity and mean-square atomic displacements are also determined in the quasi-harmonic approximation. The constant-volume heat capacity for a set of M uncoupled harmonic oscillators with frequencies ω_i is

$$C_v = \sum_{i=1}^{M}\left[\frac{\hbar^2\omega_i^2}{k^2T^2}e^{\frac{\hbar\omega_i}{kT}}(e^{\hbar\omega_i/kT}-1)^{-2}\right] \quad (2)$$

and mean-square displacement of the jth atom is

$$\langle\Delta\mu^2\rangle j = \frac{1}{Nm_j}\sum_{i=1}^{M}\left[\frac{\hbar\zeta_{ij}\zeta_{ij}^*}{\omega_i}\left(\frac{1}{2}+[e^{\frac{\hbar\omega_i}{kT}}-1]^{-1}\right)\right] \quad (3)$$

where ζ_{ij} is the vector describing the displacement of jth atom vibrating in mode i, and m_j is the mass of atom j. Both of these quantities are obtained as averages over the Brillouin zone. The constant-pressure heat capacity is obtained as the numerical derivative of the enthalpy with respect to temperature (where the enthalpy is evaluated for the structure which minimizes the free energy at that temperature).

The lattice dynamics method is used because it includes quantum mechanical effects (which are essential for determining the heat capacity) and because the Fourier space methods minimize finite system size effects. The drawback of this method is that the approximation of quasi-harmonic vibrations becomes progressively worse as the temperature approaches the melting temperature. Previous simulations have shown that this method gives good results for polyethylene up to approximately $^2/_3$ the melting temperature,[12,13] and a theoretical analysis has shown that this method is accurate for lattice parameters (but not necessarily internal atomic positions).[14]

Crystal Structures. The *n*-alkane crystals exist in several different structures, depending on the number of carbon atoms in the molecule, N, and the temperature. For *n*-alkanes with N odd and $N \geq 13$, the orthorhombic *Pbcm* structure is the thermodynamically stable crystal structure throughout most of the temperature range in which the solid state is stable.[15,16] However, the *Pbcm* structure is thermodynamically stable in only a small temperature range for *n*-alkanes with $N = 9$ and $N = 11$ [17] and is not thermodynamically stable at any temperature for *n*-alkanes with N odd and $N \leq 7$.[15] For *n*-alkanes with N even and $6 \leq N \leq 26$, the triclinic $P\bar{1}$ structure is the thermodynamically stable structure throughout most of the temperature range in which the solid state is stable.[15−17] In a small temperature range just below the melting temperarture, many of the *n*-alkane systems undergo phase transitions to other solid phases.[17,18]

The issue of the relative thermodynamic stability of the crystal structures as a function of chain length is not addressed here. A number of crystal structures are expected to have very similar free energies, such that the differences in the free energies would be less than the accuracy limits of the force field. The simulations therefore cannot reliably determine the correct thermodynamically stable structure.

The present simulations instead focus on how properties of the $P\bar{1}$ and *Pbcm* structures change with chain length. These structures were chosen because they have the most widespread ranges of thermodynamic stability for relatively short *n*-alkanes with N even and N odd, respectively. The simulations are carried out for short *n*-alkanes because the free energy evaluations become too compuationally intensive for longer *n*-alkanes (since there are 4 chains in the *Pbcm* unit cell but only 1 chain in the $P\bar{1}$ unit cell, the simulations of the $P\bar{1}$ structure can be carried out for larger N).

The present studies focus on *n*-alkanes with $5 \leq N \leq 20$. The simulations of *n*-alkanes with N even are carried out for the $P\bar{1}$ structure, which is the thermodynamically stable structure. The simulations of *n*-alkanes with N odd are carried out for the *Pbcm* structure; although *Pbcm* is not the *thermodynamically stable* structure for C_5H_{12} at any temperature or for $C_{11}H_{24}$ at low temperatures, the *Pbcm* structure is nonetheless a *metastable* structure for these systems (i.e., a free energy minimum exists for the *Pbcm* structure, but it is not the global free energy minimum).

In both the *Pbcm* and $P\bar{1}$ structures the chain axis is exactly or nearly parallel to the *c*-axis of the crystal. The two structures differ in the packing of chains perpendicular to the chain axis, as shown schematically in Figure 1: the *Pbcm* structure is based on a herringbone packing of the chains, while the $P\bar{1}$ structure is based on all chains packing with identical orientations. Note that the *Pbcm* structure consists of two layers of molecules per unit cell; the two layers are displaced relative to each other to minimize the steric interactions of adjacent chain ends.

In the limit of very long chain length, the *n*-alkane chains become polyethylene. Polyethylene usually crystallizes in an orthorhombic structure,[19] which is analogous to the *Pbcm* structure (but since the chains are infinite, there is only one layer of molecules). Polyethylene also occurs in a monoclinic structure after being stressed,[20−22] which is analogous to the $P\bar{1}$ structure (note that the monoclinic structure of polyethylene, with two chains per unit cell, is not a primitive unit cell—the primitive unit cell corresponding to this structure is a triclinic cell with one chain per unit cell, and it is this primitive unit cell that is directly comparable to the triclinic structure of the *n*-alkanes). The polyethylene unit cells consist of two CH_2 groups per chain; the axial length of two CH_2 groups can thus define the *c*-axis dimension of a polyethylene-like subcell in *n*-alkane crystals.

Results

Crystal Structures. The simulation results for the lattice parameters at zero temperature are given in Table 1. The *a* and *b* lattice parameters of the *n*-alkanes are larger than those of the corresponding polyethylene structure but approach the polyethylene values as the *n*-alkane chain length increases (the *c*-axis dimensions of the polyethylene-like subcells differ only negligibly from the value for polyethylene). The differences in these lattice parameters are due to packing effects at the chain ends (i.e., increased energy due to the steric interactions). Since longer chains are composed of a smaller proportion of chain ends, these chain-end packing effects become less significant as the chain becomes longer, and the structures of the longer *n*-alkanes approach the polyethylene structure. For the triclinic structures, the unit cell angles also trend toward those of polyethylene; note that in the long chain length limit the angle α becomes 90° and the angle β leads to the staggering of chains along the *a*-axis by half of the polyethylene intrachain repeat unit. The simulation results for the lattice parameters are compared with experimental results[19,22,23] in Table 2 (the simulation results are for the same temperatures as the experimental results); the simulation results agree with experiment to within ~2%, on average.

Thermal Expansion. The temperature dependence of the lattice parameters of the orthorhombic crystals are shown in Figure 2. The thermal expansion of all lattice parameters

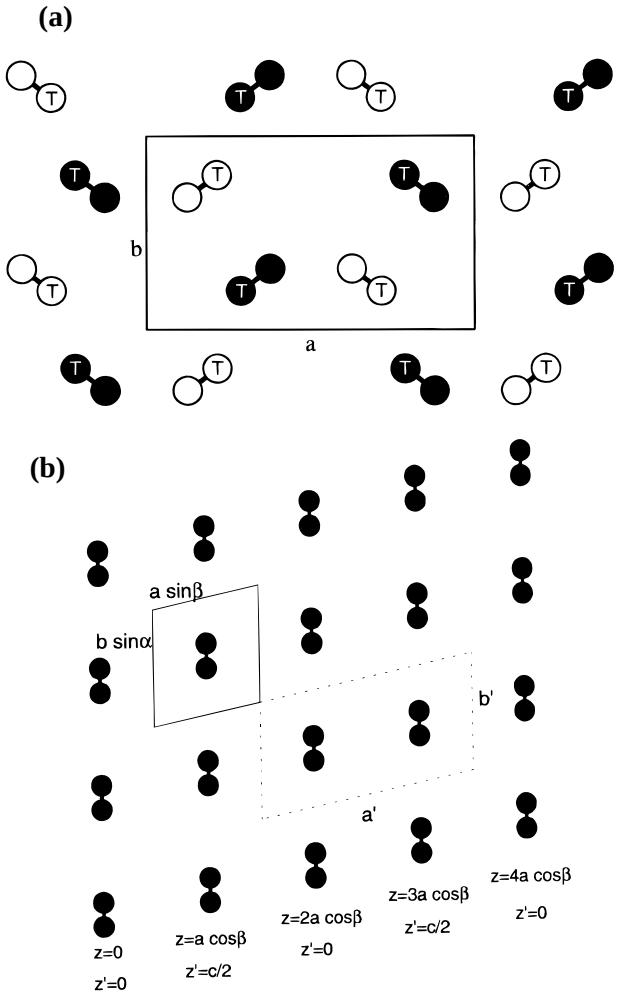

Figure 1. Crystal structures of *n*-alkane and polyethylene systems. (a) Projection along the *c*-axis of the *Pbcm* orthorhombic *n*-alkane structure. The chains are aligned along the *c*-axis, and there are 4 chains per unit cell (2 in an upper layer and 2 in a lower layer). Filled circles represent chains in the upper layer, open circles represent chains in the lower layer, and the "T" indicates the position of the terminal carbon atoms. The orthorhombic polyethylene structure is given by the filled circles only. (b) Projection along the *c*-axis of the *P*1 triclinic *n*-alkane structure. The unit cell is denoted by the solid lines. The chains are tilted with respect to the *c*-axis (not shown), and the neighboring chains along the *a*-axis are shifted along the *c*-axis by the value a cos β, as indicated by the values of *z* at the bottom of the figure. The monoclinic polyethylene structure can be described by either a monoclinic unit cell with two chains per unit cell (dashed lines and primed parameters) or a triclinic unit cell with one chain per unit cell (solid lines and unprimed parameters); the chains are aligned exactly along the *c*-axis, and the axial shifts for neighbors along the *a*-axis have the magnitude *c*/2 (note that shifts by *c* are equivalent to no shifts at all).

decreases with increasing chain length, and thermal expansion along the *c*-axis even becomes negative for long chains. The slopes of these thermal expansion curves (i.e., the thermal expansion coefficients) decrease to zero as the temperature decreases to zero, in agreement with experiment;[24,25] this decrease to zero is due to quantum mechanical effects.[11]

The trends in the thermal expansion with chain length are due to entropic effects. The thermal expansion along the *a*- and *b*-axes is driven by increases in entropy associated with increases in the *a* and *b* lattice parameters. This entropy increase arises because increases in the *a* and *b* lattice parameters allow more vibrational motion perpendicular to the chain axis (i.e., vibrational amplitudes become larger). This vibrational amplitude effect is enhanced for the atoms at the chain ends, because these

TABLE 1: Results for the Zero-Temperature Lattice Parameters of the *n*-Alkane Crystals

N	*a* (Å)	*b* (Å)	*c* (Å)	α (deg)	β (deg)	γ (deg)
			Orthorhombic			
5	7.31	4.86	16.14	90	90	90
11	7.25	4.86	31.50	90	90	90
∞	7.22	4.86	2.56	90	90	90
			Triclinic			
6	4.27	4.55	9.75	78.2	58.7	80.5
8	4.25	4.55	12.26	80.6	61.3	78.9
10	4.25	4.53	14.80	82.3	62.9	78.1
12	4.24	4.52	17.34	83.4	64.2	77.6
20	4.24	4.51	27.50	85.9	66.9	76.6
∞	4.22	4.49	2.56	90.0	72.4	76.6

TABLE 2: Comparison of the Simulation Results for the Lattice Parameters with Experiment

		a (Å)	*b* (Å)	*c* (Å)	α (deg)	β (deg)	γ (deg)
n-C_6H_{12}	exp[a]	4.17	4.70	9.71	77.4	57.0	79.2
$T = 158$ K	simulation	4.43	4.72	9.82	76.4	57.1	79.3
n-C_8H_{18}	exp[b]	4.16	4.76	12.4	80.1	62.0	75.4
$T = 173$ K	simulation	4.41	4.69	12.37	79.8	59.8	77.8
n-$C_{10}H_{22}$	exp[b]	4.31	4.81	14.9	81.6	64.7	73.5
$T = 233$ K	simulation	4.48	4.75	15.00	80.9	61.9	75.3
n-$C_{11}H_{24}$	exp[b]	7.27	4.92	31.2	90	90	90
$T = 237$ K	simulation	7.65	5.05	31.76	90	90	90
n-$C_{12}H_{26}$	exp[b]	4.30	4.79	17.42	81.3	65.6	73.8
$T = 253$ K	simulation	4.46	4.75	17.46	82.8	62.8	74.4
n-$C_{20}H_{42}$	exp[b]	4.30	4.83	27.50	86.0	68.6	72.8
$T = 291$ K	simulation	4.46	4.71	27.58	85.5	66.0	74.7
polyethylene	exp[c]	7.12	4.85	2.55	90	90	90
$T = 4$ K	simulation	7.22	4.86	2.56	90	90	90

[a] Reference 23. [b] Reference 17. [c] Reference 19.

atoms are less constrained than the atoms within the chains, as shown in Figure 3. Since longer chains are composed of a smaller proportion of chain ends, and the entropic effects which drive thermal expansion are largest at the chain ends, thermal expansion decreases with increasing chain length.

Thermal expansion along the chain axis can be considered as the sum of interchain and intrachain thermal expansions. The intrachain contribution is negative, due to the increased motions perpendicular to the chain axis which are allowed as the axial lattice parameter decreases.[26] In contrast, the interchain contribution is positive, as shown in a previous simulation of a simple model of *n*-alkane crystals.[27] For shorter chains the interchain contribution dominates, and the thermal expansion is positive. As the chain becomes longer, the intrachain contribution becomes more important, which decreases the axial thermal expansion and eventually causes the axial thermal expansion to become negative.

The thermal expansion results for the triclinic systems are analogous to those for the orthorhombic systems. The volume expansion and the volume thermal expansion coefficients of all systems, both triclinic and orthorhombic, are shown in Figure 4. The volume thermal expansion coefficients shown in this figure were obtained by first fitting the volume expansion to a second-order polynomial and then taking the analytical derivative of this polynomial. The results show that the thermal expansion coefficient decreases with increasing chain length, regardless of the crystal structure. The origins of this chain length effect are the enhanced entropic effects associated with chain ends, as discussed above.

Heat Capacity. The heat capacity at constant volume (on a per carbon basis) is shown as a function of temperature in Figure 5a. The heat capacity is found to decrease with increasing chain length. Quantum mechanical effects are clearly evident, in that

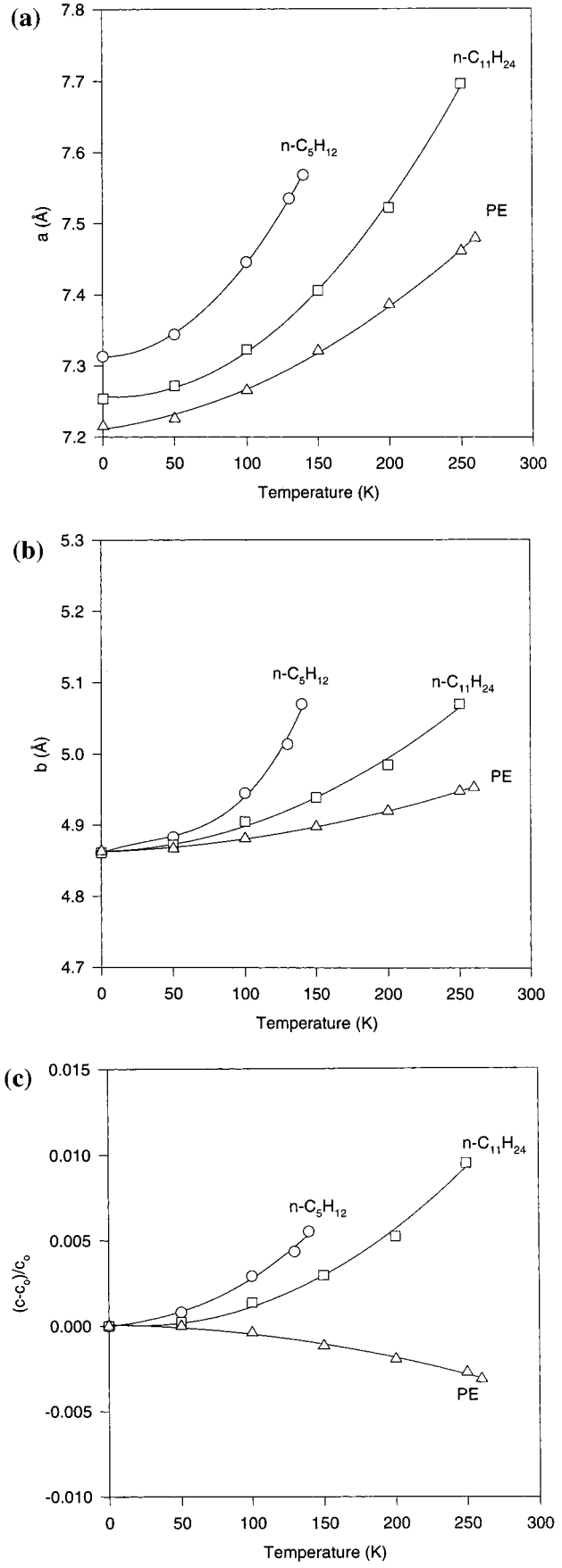

Figure 2. Temperature dependence of the lattice parameters of the orthorhombic crystals: (a) thermal expansion of the a lattice parameter; (b) thermal expansion of the *b* lattice parameter; (c) fractional thermal expansion of the *c* lattice parameter.

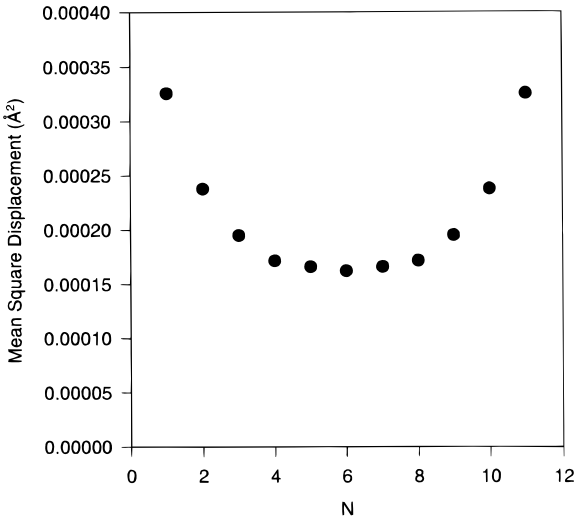

Figure 3. Mean-square displacement of the carbon atoms in *n*-$C_{11}H_{24}$ at a temperature of 150 K.

the heat capacity decreases to zero as the temperature decreases to zero. To assess the accuracy of the simulations in regard to heat capacity, the heat capacity at constant pressure is compared with experimental results for $C_{10}H_{22}$ in Figure 5b; the simulation results are in reasonable agreement with experiment,[28] although the accuracy decreases at higher temperatures due to the breakdown of the quasi-harmonic approximation.

The variations in heat capacity (per carbon atom) with chain length arise from quantum mechanical effects associated with the differing proportion of interchain modes relative to intrachain modes. For example, a system of m chains consisting of N atoms each will have $3(m - 1)$ interchain modes per $3m(N - 1)$ intrachain modes, and thus, the ratio of interchain modes to intrachain modes is $1/(N - 1)$ for large m. Since interchain modes are generally lower in frequency than intrachain modes, the interchain modes contribute more to the heat capacity due to quantum mechanical effects. Shorter chains, which have a greater proportion of interchain modes on a per carbon basis, thus have a higher heat capacity on a per carbon basis.

This effect is demonstrated for a simple one-dimensional *n*-alkane model. In this model, methyl and methylene groups are represented as united atoms, and the system consists of axially layered chains, as shown in Figure 6. The nearest-neighbor atoms within the chains interact through a strong harmonic potential (4.4 md/Å), and the nearest-neighbor atoms in different chains interact through a weak harmonic potential (0.05 md/Å). The particular system examined has 12 atoms per unit cell (with periodic boundary conditions). As the number of chains per unit cell increases from 1 to 4 (i.e., the chain length decreases), high-frequency intrachain modes convert to low-frequency interchain modes. The increase in the proportion of interchain modes with decreasing chain length leads to an increase in heat capacity as shown in Table 3.

Melting Temperature. Stable crystal structures could not be obtained above certain critical temperatures, which are shown in Figure 7 as a function of chain length. The instabilities in the *n*-alkane crystals correspond to the softening of long-wavelength vibrational modes associated with rigid motion of the chains; the modes with a wavelength approaching infinity become unstable first, and the instability then propagates to smaller wavelengths. The instability temperatures we obtain are only accurate to within approximately 10−20 K, due to difficulties associated with the free energy minimum becoming extremely shallow as the instability temperature is approached.

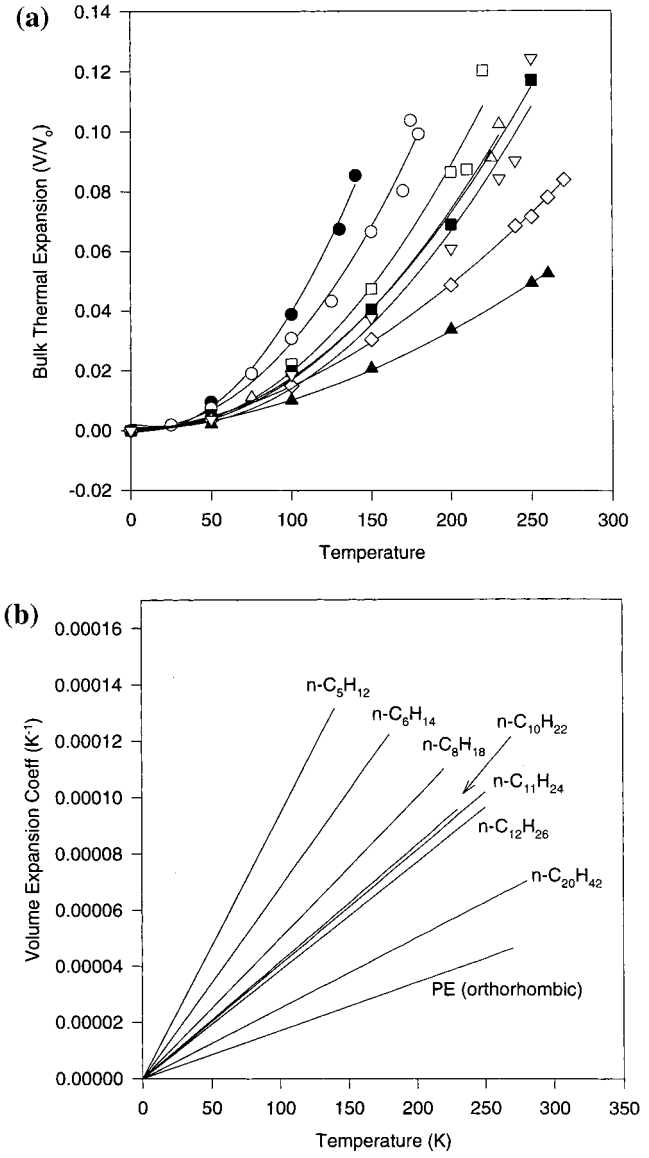

Figure 4. (a) Volume expansion. Closed circles, squares, and triangles are results for *n*-C_5H_{12}, *n*-$C_{11}H_{24}$, and orthorhombic polyethylene, respectively. Open circles, squares, up triangles, down triangles, and diamonds are results for *n*-C_6H_{14}, *n*-C_8H_{18}, *n*-$C_{10}H_{22}$, *n*-$C_{12}H_{26}$, and *n*-$C_{20}H_{42}$, respectively. (b) Volume expansion coefficient, which is equal to $(1/V)(dV/dT)$.

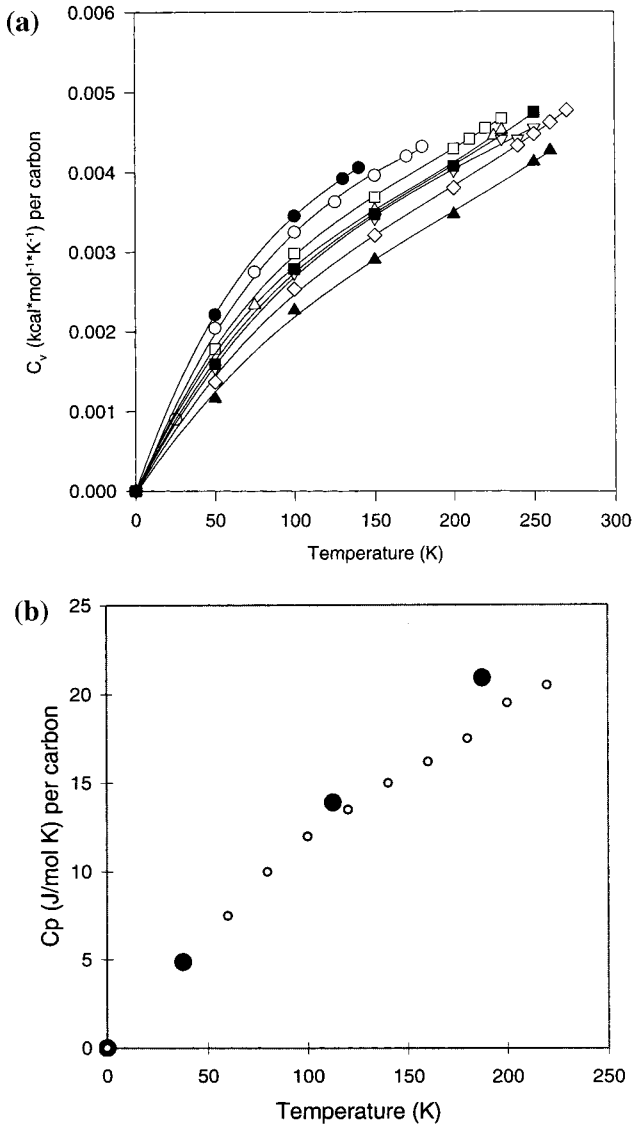

Figure 5. (a) Heat capacity at constant volume (on a per carbon basis). Symbols are the same as in Figure 4a. (b) Heat capacity at constant pressure for *n*-$C_{10}H_{22}$. Open symbols are experimental results,[28] and filled symbols are simulation results.

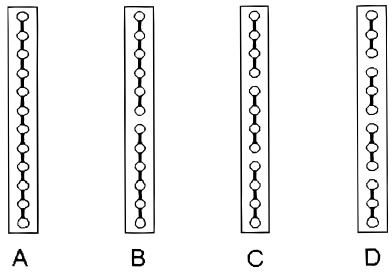

Figure 6. Four simple chain systems with 12 united atoms per unit cell and either one, two, three, and four chains in the unit cell.

Above the instability temperature there is no longer a free energy minimum corresponding to the crystal structure, which implies that a thermodynamic phase transition from the crystal to another phase must occur at or below the instability temperature. The instability temperature therefore represents an upper bound to the equilibrium phase transition temperature and limits the temperature range of metastability of the superheated crystal.[29,30] The phase transition can either be to the liquid phase or to another solid phase (such as a rotator phase). Previous results for simpler systems have shown that the instability temperatures obtained from lattice dynamics simulations correlate well with experimental melting temperatures.[31] We therefore examined the correlations between the calculated instability temperatures and the experimental melting temperatures in *n*-alkane crystals (we did not examine correlations to both the crystal-to-rotator phase transition and the melting phase transition because the difference in the temperatures for these transitions is smaller than the precision of the present results).

The instability temperatures for the *n*-alkane crystals are compared with the experimental melting temperatures[17,18,32] in Figure 7. The instability temperatures and experimental melting temperatures show the same qualitative trend and are generally within ~15 K of each other. We note that this remarkably high accuracy is most likely due to a fortuitous cancellation between the error associated with the assumption that the instability temperature corresponds to the melting temperature (which will overestimate the melting temperature), and the error associated

TABLE 3: Vibrational Frequencies (ν) of the Four Linear Systems Shown in Figure 6 and Contributions to the Heat Capacity at Constant Volume from These Vibrations at 125 K[a]

A		B		C		D	
ν (cm^{-1})	C_v (J/(mol·K))	ν (cm^{-1})	C_v (J/(mol·K))	ν (cm^{-1})	C_v (J/(mol·K))	ν(cm^{-1})	C_v (J/(mol·K))
0		0		0		0	
200	0.654	63	0.957	67	0.952	63	0.957
377	0.251	377	0.251	67	0.952	63	0.957
561	0.065	387	0.236	560	0.066	90	0.916
729	0.016	729	0.016	560	0.066	729	0.016
889	0.004	733	0.015	567	0.062	733	0.015
1031	0.001	1031	0.001	1031	0.001	733	0.015
1157	0.000	1033	0.001	1033	0.001	737	0.015
1262	0.000	1262	0.000	1033	0.001	1262	0.000
1347	0.000	1263	0.000	1347	0.000	1263	0.000
1408	0.000	1408	0.000	1347	0.000	1263	0.000
1445	0.000	1408	0.000	1347	0.000	1264	0.000

[a] Note that the intrachain vibrations are those with $\nu < 100$ cm^{-1}.

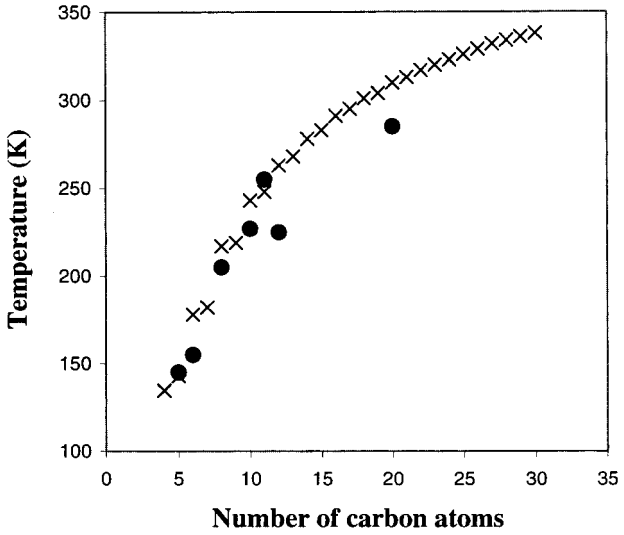

Figure 7. Simulated instability temperatures and experimental melting temperatures as a function of chain length. Closed circles are results of the present simulations, and crosses are the experimental melting temperatures ($N \leq 7$, ref 32; $8 \leq N \leq 21$, ref 17; $22 \leq N \leq 30$, ref 18).

with the quasi-harmonic approximation (which will underestimate the melting temperature).

The instability temperature obtained for the polyethylene crystal is ~270 K, which is much lower than the experimental melting temperature of ~410 K. The instability mechanisms in *n*-alkane and polyethylene crystals are different: in the *n*-alkane crystals the instabilities correspond to chains moving as rigid units, while in polyethylene crystals the instabilities correspond to intrachain buckling.[33] We believe that the force field used allows polyethylene to buckle too easily, causing the instability temperature of polyethylene to be much lower than the experimental melting temperature; however, the instabilities in the *n*-alkanes arise from a different mechanism and are thus not affected by this aspect of the force field.

Conclusions

Variations in chain length are shown to significantly influence the properties of *n*-alkane crystals. In general, the properties of *n*-alkane crystals approach the properties of polyethylene crystals as the chain length increases. The changes of the properties with chain length can be understood in terms of the changing proportion of the chain which corresponds to a chain end. Increases in chain length lead to decreases in the transverse dimensions of the unit cell, in agreement with experiment.[2,7] This effect arises from a combination of energetic effects (associated with poorer packing at the chain ends) and entropic effects (associated with the increased vibrational motion at chain ends). The constant-volume heat capacity (on a per carbon basis) decreases with increasing chain length, in agreement with the results of a simple model,[3] due to quantum mechanical effects associated with an increased proportion of lattice modes in systems with shorter chains. The temperature at which thermally induced instabilities occur in *n*-alkane systems increases with chain length and is found to correlate well with experimentally determined melting temperatures.

Acknowledgment. Funding from the National Science Foundation (Grant No. DMR-9624808), the Louisiana Board of Regents, and the donors of the Petroleum Research Fund, administered by the American Chemical Society, is gratefully acknowledged.

References and Notes

(1) Corradini, P.; Petraccone, V.; Pirozzi, B. *Eur. Polym. J.* **1983**, *19*, 299.

(2) Davis, G. T.; Eby, R. K.; Colson, J. P. *J. Appl. Phys.* **1970**, *41*, 4316.

(3) Broadhurst, M. G.; Mopisk, F. I. *J. Chem. Phys.* **1971**, *54*, 4239.

(4) Phillips, P. J. *Rep. Prog. Phys.* **1990**, *53*, 549.

(5) Flory, P. J.; Vrij, A. *J. Am. Chem. Soc.* **1963**, *85*, 3548.

(6) Crist, B. *Annu. Rev. Mater. Sci.* **1995**, *25*, 295.

(7) Davis, G. T.; Weeks, J. J.; Martin, G. M.; Eby, R. K. *J. Appl. Phys.* **1974**, *45*, 4175.

(8) Snyder, R. G.; Strauss, H. L.;Alamo, R.; Mandelkern, L. *J. Chem. Phys.* **1993**, *100*, 5422.

(9) Palmo, K.; Mirkin, N. G.; Krimm, S. *J. Phys. Chem.*, submitted for publication.

(10) Karasawa, N.; Goddard, W. A. *J. Phys. Chem.* **1989**, *93*, 7320.

(11) Ashcroft, N. W.; Mermin, N. D. *Solid State Physics*; Saunders College Press: Philadelphia, PA, 1976.

(12) Lacks, D. J.; Rutledge, G. C. *J. Phys. Chem.* **1994**, *98*, 1222.

(13) Rutledge, G. C.; Lacks, D. J.; Martonak, R.; Binder, K. *J. Chem. Phys.* **1998**, *108*, 10274.

(14) Allan, N. L.; Barron, T. H. K.; Bruno, J. A. O. *J. Chem. Phys.* **1996**, *105*, 8300.

(15) Norman, N.; Mathisen, H. *Acta Chem. Scand.* **1972**, *26*, 3913.

(16) Craig, S. R.; Hastie, G. P.; Roberts, K. J.; Sherwood, J. A. *J. Mater. Chem.* **1994**, *4*, 977.

(17) Espeau, P.; Robles, L.; Mondieig, D.; Haget, Y.; Cuevas-Diarte, M. A.; Oonk, H. A. J. *J. Chim. Phys.* **1996**, *93*, 1217.

(18) Sirota, E. B.; Singer, D. M. *J. Chem. Phys.* **1994**, *101*, 10873.

(19) Avitabile, G.; Napolitano, R.; Pirozzi, B.; Rouse, K. D.; Thomas, H. W.; Wills, B. T. M. *J. Polym. Sci., Polym. Lett. Ed.* **1975**, *13*, 351.

(20) Kiho, H.; Peterlin, A.; Geil, P. H. *J. Appl. Phys.* **1964**, *35*, 1599.

(21) Takahashi, Y.; Ishida, T. *J. Polym. Sci. B* **1988**, *26*, 2267.

(22) Seto, T.; Hara, T.; Tanaka, K. Japan. *J. Appl. Phys.* **1968**, *7*, 31.
(23) Norman, N.; Mathisen, H. *Acta Chem. Scand.* **1961**, *15*, 1755.
(24) White, G. K.; Choy, C. L. *J. Polym. Sci., Polym. Phys. Ed.* **1984**, *22*, 835.
(25) Engeln, I.; Meissner, M.; Pape, H. E. *Polymer* **1985**, *26*, 364.
(26) Kobayashi, Y.; Keller, A. *Polymer* **1970**, *11*, 114.
(27) McGann, M. R.; Lacks, D. J. *J. Chem. Phys.* **1998**, *108*, 2622.
(28) Dainton, F. S.; Evans, D. M.; Hoare, F. E.; Melia, T. P. *Polymer* **1962**, *3*, 277.
(29) Wang, J.; Li, J.; Yip, S.; Wolf, D.; Phillpot, S. *Physica A* **1997**, *240*, 396.
(30) Phillpot, S. R.; Lutsko, J. F.; Wolf, D.; Yip, S. *Phys. Rev. B* **1989**, *40*, 2831; Lutsko, J. F.; Wolf, D.; Phillpot, S. R.; Yip, S. *Phys. Rev. B* **1989**, *40*, 2841.
(31) Boyer, L. L. *Phys. Rev. Lett.* **1979**, *42*, 584; Boyer, L. L. *Phys. Rev. Lett.* **1980**, *45*, 1858.
(32) *CRC Handbook of Chemistry and Physics*; CRC Press: West Palm Beach, FL, 1978.
(33) McGann, M. R,; Lacks, D. J. *Phys. Rev. Lett* **1999**, *82*, 952.